PHILOSOPHICAL TRANSACTIONS OF THE ROYAL SOCIETY A MATHEMATICAL, PHYSICAL & ENGINEERING SCIENCES

Direct measurement of tissue blood flow and metabolism with diffuse optics

Rickson C. Mesquita, Turgut Durduran, Guoqiang Yu, Erin M. Buckley, Meeri N. Kim, Chao Zhou, Regine Choe, Ulas Sunar and Arjun G. Yodh

Phil. Trans. R. Soc. A 2011 **369**, 4390-4406
doi: 10.1098/rsta.2011.0232

PHILOSOPHICAL TRANSACTIONS OF THE ROYAL SOCIETY A

Phil. Trans. R. Soc. A (2011) **369**, 4390–4406
doi:10.1098/rsta.2011.0232

Direct measurement of tissue blood flow and metabolism with diffuse optics

By Rickson C. Mesquita[1,2,*], Turgut Durduran[3], Guoqiang Yu[4], Erin M. Buckley[1], Meeri N. Kim[1], Chao Zhou[5], Regine Choe[6], Ulas Sunar[7] and Arjun G. Yodh[1]

[1]*Department of Physics and Astronomy, University of Pennsylvania, Philadelphia, PA 19104, USA*
[2]*Institute of Physics 'Gleb Wataghin', University of Campinas – UNICAMP, Campinas, SP 13083–859, Brazil*
[3]*ICFO – Institut de Ciències Fotòniques, Mediterranean Technology Park, Castelldefels, Barcelona 08860, Spain*
[4]*Center for Biomedical Engineering, University of Kentucky, Lexington, KY 40506, USA*
[5]*Department of Electrical Engineering and Computer Science and Research Laboratory of Electronics, Massachusetts Institute of Technology, Cambridge, MA 02139, USA*
[6]*Department of Biomedical Engineering, University of Rochester, Rochester, NY 14642, USA*
[7]*Department of Cell Stress Biology and PDT Center, Roswell Park Cancer Institute, Buffalo, NY 14263, USA*

Diffuse optics has proven useful for quantitative assessment of tissue oxy- and deoxyhaemoglobin concentrations and, more recently, for measurement of microvascular blood flow. In this paper, we focus on the flow monitoring technique: diffuse correlation spectroscopy (DCS). Representative clinical and pre-clinical studies from our laboratory illustrate the potential of DCS. Validation of DCS blood flow indices in human brain and muscle is presented. Comparison of DCS with arterial spin-labelled MRI, xenon-CT and Doppler ultrasound shows good agreement ($0.50 < r < 0.95$) over a wide range of tissue types and source detector distances, corroborating the potential of the method to measure perfusion non-invasively and *in vivo* at the microvasculature level. All-optical measurements of cerebral oxygen metabolism in both rat brain, following middle cerebral artery occlusion, and human brain, during functional activation, are also described. In both situations, the use of combined DCS and diffuse optical spectroscopy/near-infrared spectroscopy to monitor changes in oxygen consumption by the tissue is demonstrated. Finally, recent results spanning from gene expression-induced angiogenic response to stroke care and cancer treatment monitoring are discussed.

*Author for correspondence (rickson@sas.upenn.edu).

One contribution of 20 to a Theo Murphy Meeting Issue 'Illuminating the future of biomedical optics'.

Collectively, the research illustrates the capability of DCS to quantitatively monitor perfusion from bench to bedside, providing results that match up both with literature findings and with similar experiments performed with other techniques.

Keywords: diffuse correlation spectroscopy; blood flow; cerebral blood flow; oxygen metabolism; brain; cancer

1. Introduction and background

The focus of this paper is centred on measurement of blood flow in deep tissues with diffusing near-infrared (NIR) light. The paper is not intended as a comprehensive review; rather, we aim to provide a self-contained and personal perspective of the field using examples from our laboratory. The reader will gain insight about fundamental ideas that underpin the method, appreciation for the importance of measuring deep tissue blood flow and specific knowledge about how this general experimental approach can have an impact in clinical and pre-clinical contexts. Interested readers are encouraged to consult primary papers for more detail, as well as useful reviews [1–4] and references therein.

The diffuse light correlation techniques are built upon dynamic light-scattering concepts. The original 'dynamic light scattering' or 'quasi-elastic light scattering' techniques [5–8] recorded temporal fluctuations of light intensity scattered from a sample in order to learn about the motions of sample constituents, e.g. the Brownian dynamics of suspended colloidal particles or macromolecules. In typical single-scattering measurements, illuminated particles re-radiate incident light into many directions and the re-radiated light travelling along one direction is detected; when particles move, the relative phases of the collected re-radiated signals will vary and the detected light intensity fluctuates. Typically, when particles move through distances of the order of the wavelength of light, the collected signals are observed to fluctuate significantly. Information about these particle motions is derived from the scattered light electric field temporal autocorrelation function (or its Fourier transform).

The simple dynamic light-scattering method does not work when samples become turbid and incident light fields are multiply scattered. In practice, one can carry out the same temporal autocorrelation function measurements described above; however, inversion of correlation function data to recover quantitative information about scatterer motion is non-trivial in the multiple-scattering limit. Thus, direct application of the method to biological tissue is challenging.

Of course, similar challenges were faced by researchers aiming to carry out absorption spectroscopy of tissue, and these challenges were surmounted by modelling light transport through tissue as a diffusion problem. The diffusion approximation enabled experimenters to quantitatively understand the trajectory of light through tissue and then to 'effectively reset' the pathlengths employed in the traditional absorption spectroscopy measurement to new, tissue-scattering-dependent values. In a similar spirit, one can envision the electric field temporal autocorrelation function propagating through tissue, scattering from small volume elements within the sample and then propagating ballistically, then scattering again, etc., all in a random manner as the photons travel from one side of the tissue sample to a tissue surface (figure 1*a*). A key

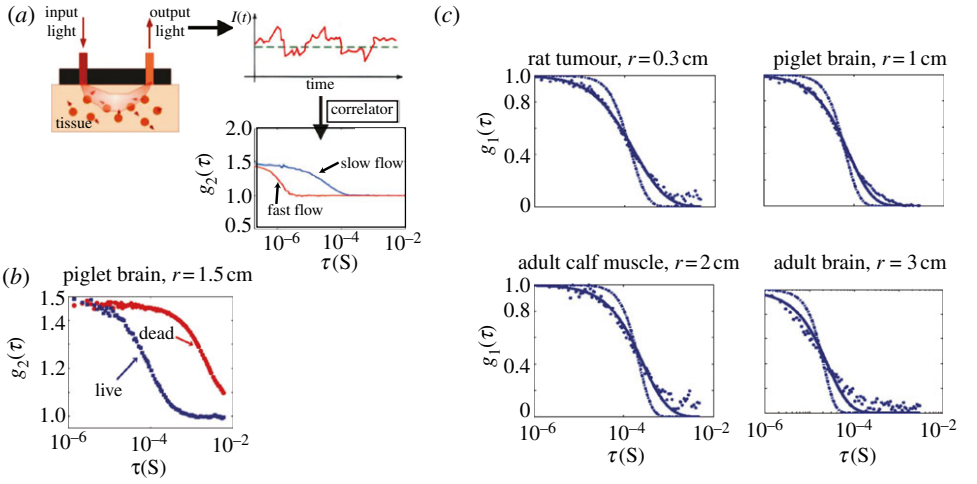

Figure 1. (*a*) Schematic of the DCS measurement. The light intensity detected at the output fibre fluctuates in time and is fed to an autocorrelator device that computes the normalized temporal *intensity* autocorrelation function ($g_2(\tau)$) from photon arrival times. (*b*) Temporal *intensity* autocorrelation curves measured in the brain of a piglet (living and dead). (*c*) Examples of normalized temporal electric *field* autocorrelation curves ($g_1(\tau)$) across a wide variety of biological animal and human tissues in their normal states, along with the Brownian (solid lines) model and random-flow (dashed-dotted lines) model best fits for $\langle \Delta r^2(\tau) \rangle$ (dots, raw data). The Brownian model fits the data better than the random-flow model ($\boldsymbol{r}$ refers to source–detector separation). (Online version in colour.)

steady-state mathematical equation governing the transport of electric field temporal autocorrelation through tissue is given below, i.e. the correlation diffusion equation [9,10]

$$\nabla \cdot (D(\boldsymbol{r}) \nabla G_1(\boldsymbol{r}, \tau)) - v \left(\mu_a(\boldsymbol{r}) + \frac{\alpha}{3} \mu_s' k_0^2 \langle \Delta r^2(\tau) \rangle \right) G_1(\boldsymbol{r}, \tau) = v S(\boldsymbol{r}, t). \qquad (1.1)$$

Here, $G_1(\boldsymbol{r}, t) = \langle \boldsymbol{E}^*(\boldsymbol{r}, t) \boldsymbol{E}(\boldsymbol{r}, t + \tau) \rangle$ is the unnormalized temporal electric field ($\boldsymbol{E}(\boldsymbol{r}, t)$) autocorrelation function in the medium at position $\boldsymbol{r}$ and time t; τ is the autocorrelation function time delay, and the brackets represent time and/or ensemble averages. $D \cong 1/(3\mu_s')$ is the light diffusion coefficient in the medium; μ_a is the absorption coefficient; μ_s' is the reduced scattering coefficient (i.e. the inverse of the photon random walk step-length); v is the speed of light in the medium, and $S(\boldsymbol{r}, t)$ represents the light source.

The primary new features of the correlation diffusion equation compared with the conventional steady-state light diffusion equation (obtained from equation (1.1) by letting the autocorrelation time, τ, approach zero) are associated with particle motion: α represents the fraction of photon-scattering events that occur from moving particles in the medium (e.g. red blood cells; RBCs); $\langle \Delta r^2(\tau) \rangle$ is the mean-square particle displacement in time τ (i.e. in tissue, the mean-square displacement factor could characterize the motions of RBCs in the tissue vasculature); $k_0 = 2\pi/\lambda$ is the wavenumber of the light diffusing through the medium. Diffuse correlation spectroscopy (DCS) refers to the measurement of the diffusing temporal field autocorrelation function to obtain information about

tissue dynamics. Equation (1.1) is essentially a differential equation formulation of diffusing wave spectroscopy (DWS) [11–13], a technique developed earlier in the soft condensed matter community for studies of a variety of highly scattering complex fluids. DCS, as formulated above, is better suited than DWS (which essentially dealt with homogeneous turbid media) for handling point sources, heterogeneous media and as a starting formulation for correlation tomography in tissue.

As is the case for traditional dynamic light scattering, the *intensity* autocorrelation function is usually measured by the experimenter, rather than the *field* correlation function. The Siegert relation [14] links these two correlation functions. It can be used to relate measurements of the intensity autocorrelation function to the theory for the electric field autocorrelation function, without direct measurement of phase information,

$$g_2(\tau) = 1 + \beta |g_1(\tau)|^2. \tag{1.2}$$

Here, $g_1(\tau)$ and $g_2(\tau)$ are the normalized autocorrelation functions for the electric field and intensity, respectively; β is a coherence factor, which is mainly determined by the optical detection system, and it should be close to unity for an ideal experimental set-up and is often one-half in our measurements. Typically, best fits to either $g_1(\tau)$ or $g_2(\tau)$ are employed to derive a best estimate for the dynamical tissue factor, $\alpha\langle\Delta r^2(\tau)\rangle$.

The precise physiological origin of the factor, $\alpha\langle\Delta r^2(\tau)\rangle$, is not well understood. Much of the experimental evidence suggests that DCS, like near-infrared spectroscopy (NIRS, also called diffuse optical spectroscopy; DOS), is most sensitive to the physiology in the *microvasculature* (i.e. capillaries, arterioles and venules). In fact, DCS shares many of the light penetration and modelling advantages of NIRS, but it provides a qualitatively different physiological signal. In NIRS, the signal is related to the haemoglobin concentration changes via optical absorption [1,15–17]. By contrast, the DCS signal is due to the motion of scatterers in the tissue (i.e. RBCs); therefore, DCS provides a rather direct measure of blood flow. Although no significant cross-talk between NIRS and DCS has been observed, large changes in the blood volume (proportional to the sum of oxy- and deoxyhaemoglobin concentrations) will change the fraction of photon-scattering events, α, therefore affecting the product, $\alpha\langle\Delta r^2(\tau)\rangle$. Such effects will be small and can be accounted for by independent NIRS/DOS measurements. For the mean-square particle displacement, in practice, the Brownian model, $\langle\Delta r^2(\tau)\rangle = 6D_{\mathrm{B}}\tau$, fits the observed correlation decay curves fairly well over a wide range of tissue types and source–detector separations, including rat brain [18–22]; mouse tumours [23–26]; piglet brain [27]; and human skeletal muscle [28–32], human tumours [33–39] and human brain [40–48] (figure 1*c*). Here, D_{B} is an *effective* diffusion coefficient that is a few orders of magnitude larger than the traditional thermal Brownian diffusion coefficient of cells in blood given by the Einstein–Smoluchowski relation [49]. Use of the Brownian model is hardly satisfying. In fact, RBCs in the microvasculature do not move purely ballistically or diffusively; they experience position-dependent shear stresses and hydrodynamic interactions, and they roll, tumble and translate through the vasculature. The Brownian model provides a convenient approximation for data fitting and for defining a blood flow index ($\mathrm{BFI} \equiv \alpha D_{\mathrm{b}}$) from the DCS measurement. The BFI is not a measure of absolute blood flow in the strict

Table 1. All *in vivo* DCS validation studies published to date. ASL-MRI, arterial spin-labelled MRI; PDT, photodynamic therapy.

sample	perturbation	modality	correlation coefficient	slope DCS/mod	references
mouse	femoral artery occlusion	laser Doppler	>0.8	0.96–1.07	[50]
mouse tumour	antivascular therapy	contrast-enhanced ultrasound	n.a.	agreement	[24]
mouse tumour	PDT	Doppler ultrasound	n.a.	agreement	[25]
mouse tumour	PDT	power Doppler ultrasound	n.a.	0.97	[26]
rat	hypercapnia	ASL-MRI	0.81–0.86	0.75	[22]
rat	hypocapnia	laser Doppler	0.94	1.3	[51]
neonatal piglet	traumatic brain injury	fluorescent microspheres	0.63	0.4	[27]
premature neonates	absolute baseline	transcranial Doppler	0.53	n.a.	[48]
term neonate	hypercapnia	ASL-MRI	0.7	0.85	[52]
premature infant	absolute baseline	transcranial Doppler	0.91	0.9	[53]
human muscle	cuff inflation/deflation	ASL-MRI	>0.77	1.5–1.7	[29]
adult human	pressors and hyperventilation	xenon-CT	0.73	1.1	[54]
adult human	acetazolamide	transcranial Doppler	n.a.	agreement	[46]

sense (e.g. it has the wrong units), but the relative change in BFI (i.e. rBFI) has been repeatedly shown (table 1) to be a quantitative measure of relative changes in blood flow (rBF) [1,3,22,27,29,46].

The complete details of a typical DCS experimental set-up can be found elsewhere [2–4]. Briefly, a narrowband continuous wave (CW) diode laser in the NIR range with long coherence length (i.e. greater than 20 m) is used as the light source. The light beam is delivered to the tissue through an optical fibre, with an output power of approximately 10–25 mW. The light-intensity fluctuations within a single speckle area are detected using a single-mode fibre and a fast single photon-counting device (e.g. an avalanche photo-diode). Finally, an autocorrelator takes the detector output and uses photon arrival times to compute the light-intensity temporal autocorrelation function. The integration time for generating a reliable curve depends on source–detector separation, etc., but typically varies from 1 to 3 s. Since single-mode fibres are employed for detection, the detection area is small and achieving a high signal-to-noise ratio (SNR) is challenging at the largest source–detector separations. Besides the laser power and the integration time, the SNR also depends on the source–detector distance, ρ. For small animals such as mice and rats, in which $0.3 \leq \rho \leq 1.2$ cm, the SNR can be as high as 100, with a photon counting superior to 500 kHz. For brain human experiments, on the other hand, large source–detector distances

are desirable to separate cortical responses from scalp and skull responses. Since the mean photon depth sensitivity is approximately one-third to one-half of the distance between a source and a detector [55], separations of 2.5 cm or more on the surface of the human head are needed to probe the cerebral cortex. These large separations limit the SNR for a *single* detection fibre to vary from 2 to 10 in most cases (i.e. corresponding to photon counting rates of 10–100 kHz). In these cases, by averaging over many trials and/or a population sample, or by averaging over many detection fibres, it is possible to further improve measurement SNR and derive meaningful results in the human brain.

Before moving to the validation section, we briefly consider the current state of the field in relation to practical application. The ability to measure tissue haemodynamics and haemodynamic responses to stimuli is important for many clinical and pre-clinical problems, including brain pathology and tumour detection/characterization. Diffuse optical tomographic (DOT) and spectroscopic (DOS/NIRS) methods have been demonstrated to measure tissue blood volume, blood oxygenation and changes thereof, in both research and clinical settings. In some cases, one can obtain information about blood flow with DOS, but this information is derived indirectly [56,57]. The development of DCS now enables clinicians to measure several haemodynamic parameters independently with non-invasive optical probes (i.e. haemoglobin concentrations by DOS/NIRS and *blood flow* by DCS). This development opens up the possibility for monitoring *oxygen metabolism*. Furthermore, even without the benefit of DOS/NIRS, DCS can provide important information about microvascular blood flow that is often of interest in its own right. Translation of DCS methods into the clinic holds potential for spectacular future pay-offs. Thus, although our microscopic understanding of tissue DCS signals is incomplete, it remains worthwhile to push forward to discover the physiological scenarios, wherein DCS can be used fruitfully.

2. Flow validation

In §1, we defined a $\mathrm{BFI} = \alpha D_\mathrm{b}$, which approximately accounts for the fraction of scattering events from moving scatterers (α) and the motion (D_b) of the scatterers. A best-fit to the DCS temporal light intensity (or electric field) autocorrelation function provides an estimate for BFI. An example of the dependence of the BFI on the factor α is shown in figure 2. In this experiment, the concentration of RBCs around the femoral artery/vein was manipulated by injection of diluted blood. Under normal conditions (i.e. no injection), the BFI was measured to be $2.5 \times 10^{-8}\,\mathrm{cm^2\,s^{-1}}$. The introduction of diluted blood (i.e. RBC concentration effectively reduced by a factor of approx. 10) lowered the concentration of RBCs in the femoral artery, while a pump kept the circulation speed approximately constant. The measured BFI decreased by a factor of 7 as a result, thereby providing quantitative evidence that BFI is sensitive to the number density of moving scatterers (RBCs) in the tissue. (Note that differences in RBC motions are also influenced by RBC concentration via viscosity effects.)

Validation of DCS in the clinic has begun relatively recently [32–38, 52–54, 58]. Figure 3 exhibits one example. In this case, DCS measurements of cerebral blood flow (CBF) are compared with flow measurements obtained by xenon-CT in

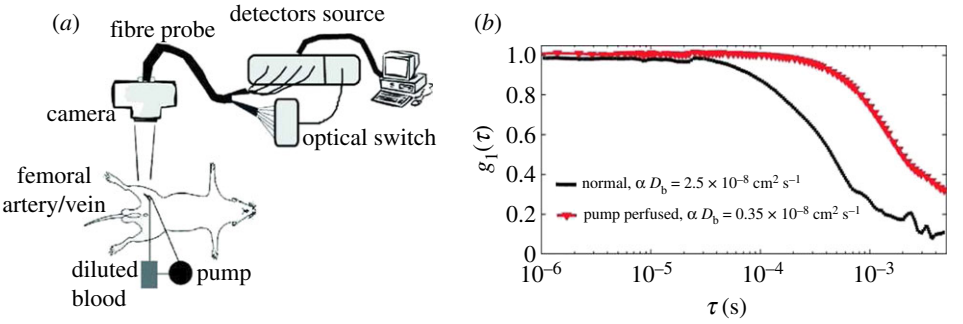

Figure 2. (*a*) Experimental schematic: blood was diverted to a pump and reservoir and then re-injected into the femoral artery. DCS data from the flow through the leg vasculature were acquired using a non-contact camera probe. (*b*) Temporal electric field autocorrelation curves obtained before (labelled as 'normal') and during the pump-perfused scenario. Blood was diluted by approximately 10 times in the pump-perfused measurement (modified from [1]). (Online version in colour.)

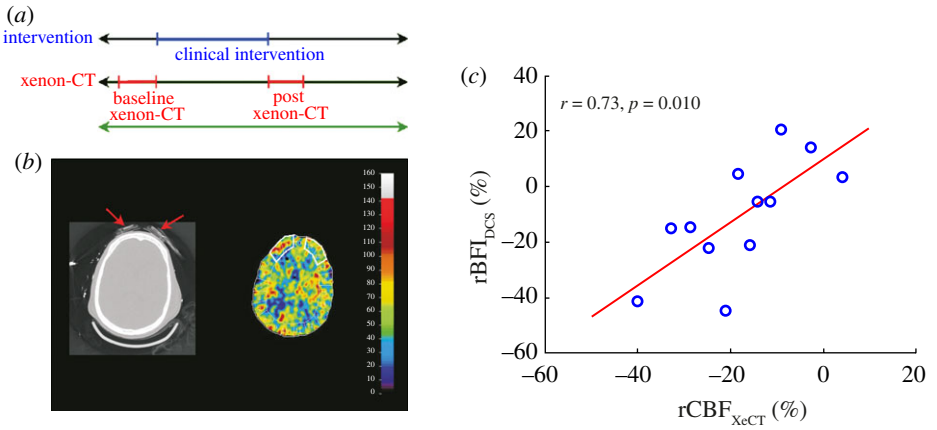

Figure 3. (*a*) Experimental protocol showing the timing of the two flow measurement techniques and the clinical intervention. (*b*) Left: anatomical map showing the position of the optical probe on the head. Right: CBF map obtained from a xenon-CT scan after Xe infusion. (*c*) Correlation between CBF as measured by DCS and xenon-CT (modified from [54]). (Online version in colour.)

brain-injured patients in the neuro-intensive care unit [54]. Although it is a current clinical 'standard of care' flow measurement, xenon-CT is an invasive technique and is not suitable for continuous bedside monitoring. In this study, we used xenon-CT images of the same tissue volumes covered by our DCS probes, and we compared rBF changes during various regular interventions in the neuro-intensive care unit, such as increased dose of vasopressor drugs (i.e. agents that cause constriction of blood vessels, leading to an increase in blood pressure). The blood flow changes obtained from both techniques were quite strongly correlated, i.e. a correlation coefficient of $r = 0.73$ was obtained for eight subjects (figure 3).

A second DCS validation example was performed with very low birth-weight preterm infants [53]. The skull anatomy of this patient population permits us to probe a significant fraction of the cortex. Briefly, in this study, we compared

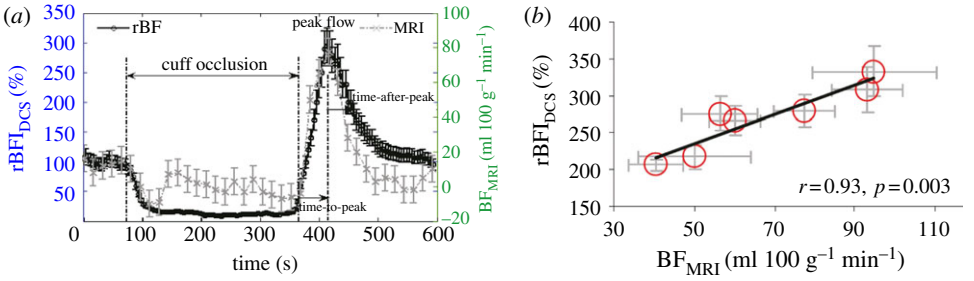

Figure 4. (*a*) Temporal time course of rBF measured by DCS (left axis) and MRI (right axis) during a cuff occlusion experiment. (*b*) Quantitative correlation between the two techniques based on peak flow (modified from [29]). (Online version in colour.)

microvascular CBF, measured with DCS, with macrovascular blood velocity in the middle cerebral artery, measured with transcranial Doppler ultrasound (TCD), a technique routinely used in the clinic. The absolute BFI obtained by DCS was quite well correlated with peak systolic velocity measured by TCD ($r = 0.76$). Although not fully understood, the evidence points towards a relationship between microvasculature perfusion in brain tissue and flow velocity in the middle cerebral artery.

Finally, a third comparison of DCS with an established flow-imaging modality, arterial spin-labelled perfusion MRI (ASL-MRI), is exhibited in muscle tissue [29]. Figure 4 shows the temporal dynamics of tissue perfusion during cuff inflation and deflation over the human calf muscle using DCS and ASL-MRI. Cuff inflation is a standard paradigm to create a brief period of ischaemia and hyperaemic response; the scheme induces a strong drop in blood flow followed by a large overshoot immediately after deflation. Flow responses measured by the two techniques in the same tissue region were compared. The overall temporal behaviour reported by the two techniques was highly correlated. Peak flow variations during hyperaemia were also significantly correlated, providing quantitative blood flow validation of the DCS method in muscle tissue.

3. Brain function and oxygen metabolism

An important area of application of diffuse optical methods concerns brain function and physiology. Many well-known functional paradigms can be applied to explore the normal responses associated with specific brain areas, such as vision in the occipital cortex, motor skills in the somatomotor cortex and verbal fluency in temporal and frontal areas. A functional paradigm typically induces an increase of neuronal communication in a specific region of the brain. This increased neuronal activity, in turn, initiates a chain of processes that ultimately produces changes in the vasculature response and haemoglobin concentration. This interaction between 'electrical' and 'haemodynamic' activity is called neurovascular coupling. Neurovascular coupling is responsible for converting changes in neuronal activity into metabolic and vascular responses in the brain.

While tissue function is often manifested in haemodynamic signatures that can be measured with DOS/NIRS and DCS, the interpretation of these haemodynamic-dependent techniques can be complicated because of competing

effects during brain activation, and because of lack of information about the relationships between evoked neuronal, metabolic and vascular responses. The interplay between vascular supply, tissue oxygen consumption and regulatory effects, although greatly debated, remains poorly understood. Clearly, more comprehensive sets of haemodynamic data containing independent information about haemoglobin concentration, blood oxygenation and blood flow are desirable.

The measurement of changes in all three of these haemodynamic parameters permits experimenters to compute changes in another fundamental tissue property: oxygen metabolism. The cerebral metabolic rate of oxygen ($CMRO_2$) is related to CBF, to arterial oxygen concentration ($[O_2]_a$) and to the oxygen extraction fraction (OEF) by Fick's law [19,59,60]

$$CMRO_2 = OEF \cdot CBF \cdot [O_2]_a. \tag{3.1}$$

OEF is defined as the fractional conversion of oxygen concentration from arterioles to venules. By assuming a compartment model in which the optical signal originates from a mixture of arterial, capillary and venous blood, it is possible to write the OEF in terms of both the arterial and tissue oxygen saturations [19],

$$OEF = \frac{(S_aO_2 - S_tO_2)}{(\gamma S_aO_2)}. \tag{3.2}$$

Typically, S_aO_2 is either assumed constant or obtained from blood gas measurements, and γ indicates the percentage of blood volume contained in the venous compartment of the vascular system, while S_tO_2 is obtained from DOS/NIRS. For relative changes, and under the assumption of constant compartmentalization, the factor γ divides out. Then, assuming that $[O_2]_a$ remains constant, the calculation of relative changes of $CMRO_2$ ($rCMRO_2$) gives

$$rCMRO_2 = \frac{CMRO_2(t)}{CMRO_2(t_0)} = \frac{CBF(t)}{CBF(t_0)} \cdot \frac{[S_aO_2(t) - S_tO_2(t)]}{[S_aO_2(t_0) - S_tO_2(t_0)]} \cdot \frac{S_aO_2(t_0)}{S_aO_2(t)}. \tag{3.3}$$

As DOS/NIRS can be used measure S_tO_2, and, therefore, to provide a measure OEF through equation (3.2), and as DCS measures CBF, tissue oxygen metabolism (especially relative changes in oxygen metabolism) can be derived from information available to all the optical methods.

The use of combined DCS and DOS/NIRS to monitor changes in $CMRO_2$ was demonstrated in both animal and humans by our group [18,19,40,52]. The first demonstration of combined DCS and DOS/NIRS to monitor concurrent flow and oxygenation changes in brain was carried out in a pre-clinical rat model during hypercapnia [18]. The first *in vivo* all-optical demonstrations of the measurement of $CMRO_2$ (again, employing concurrent DCS and DOS/NIRS) was subsequently carried out in both animals [19] and humans [40]. The utility of the technique for measurement of relative changes in $CMRO_2$ (i.e. $rCMRO_2$) is shown in figure 5. In this work, variation of haemodynamic parameters was monitored during temporary focal cerebral ischaemia in rats. By occluding the middle cerebral artery over 60 min, average blood flow in the ischaemic region across five rats dropped by 58 (±4)%, while OEF increased by approximately 39 (±6)%. This interplay combined to induce a decrease in $CMRO_2$ of 59 (±7)% from its baseline

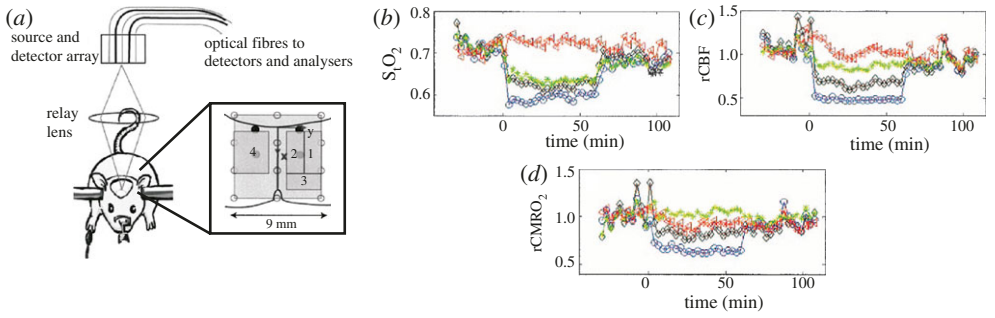

Figure 5. (*a*) Schematic showing the experimental optical probe with two detectors and nine sources. The regions of interest (ROIs) on the brain are shown in the box, and they were defined relative to the bregma: ROI-1 is an ischaemic region, ROI-2 is a peri-ischaemic region towards midline, ROI-3 is a posterior peri-ischaemic region and ROI-4 is a contralateral control region. (*b*) Time traces of S_tO_2, CBF and $CMRO_2$ in the four ROIs; blue, black, green and red represent ROI-1, 2, 3 and 4, respectively; $t = 0$ represents the beginning of the artery occlusion (modified from [19]). (Online version in colour.)

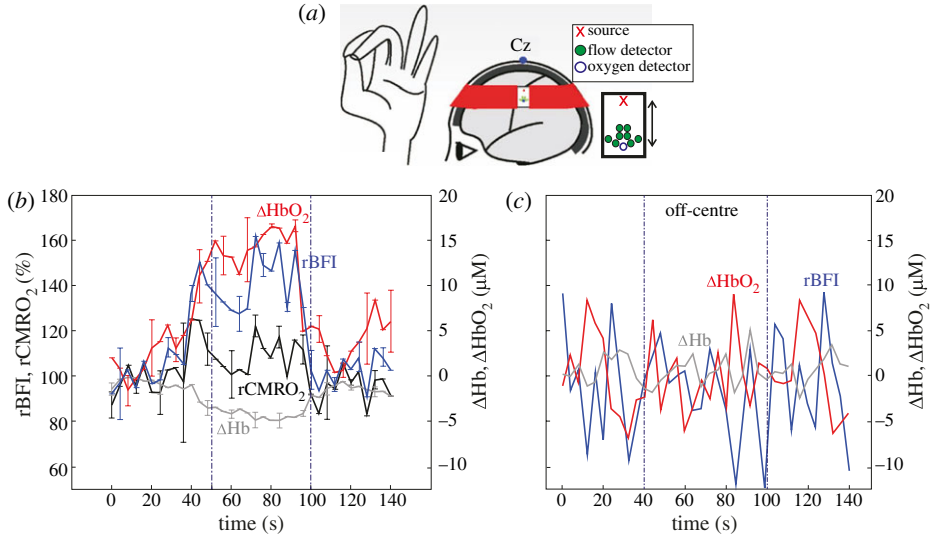

Figure 6. (*a*) Schematic showing the experimental finger tapping activation set-up. (*b*) Data ($n = 5$) with the probe located over the somatomotor cortex, and (*c*) 1 cm off-centre from the activation spot (modified from [40]). (Online version in colour.)

in the most strongly affected tissue. Haemodynamic and metabolic changes in the contralateral side of the occlusion showed slight (but not significant) decreases compared with baseline.

More recently, we investigated haemodynamic and metabolic responses associated with finger tapping activation non-invasively *in vivo*, through the skull [40]. The observations are summarized in figure 6. With the probe placed directly over the motor activation site, we observed large perturbations in the

concentrations of oxyhaemoglobin, deoxyhaemoglobin and CBF. Averaging over a small subject population permitted calculation of oxygen metabolism with relatively good SNR. In addition, when the probe was positioned 1 cm off-centre from the motor cortex, no significant changes were observed, indicating that (i) the changes seen at the motor cortex were due to motor activation and (ii) the functional changes are very well localized in the brain. These results matched up quantitatively with similar experiments performed with other functional neuroimaging techniques, such as MRI and positron emission tomography (PET) [61–63]. Since this early research, many different functional activation paradigms have been studied with diffuse optics [41–47]. As noted above, the addition of DCS is critical, because it unambiguously permits quantification of changes in oxygen metabolism in all of these experiments.

4. Clinical and pre-clinical applications of diffuse correlation spectroscopy

Beyond validation, $CMRO_2$ and functional activation applications, research in the field has focused on clinical experiments aiming to improve patient care and on pre-clinical experimentation which provides insight about cancer therapy, and so on. Most current clinical methods focus on metabolism-related problems and issues with cerebral autoregulation. In fact, many treatment strategies for brain-injured patients aim to increase blood flow to the injured parts of the brain. Current diagnostic tools available to clinicians are either very invasive (e.g. intracranial pressure, oxygen monitors, etc.), or are not continuous and are expensive (e.g. MRI, Xe-CT, etc.). Therefore, a niche exists for portable, non-invasive, diffuse optical methods at the bedside.

One such example is in the care of acute ischaemic stroke (AIS) patients. In this case, optimization of CBF is a major sub-goal for salvaging as much of the ischaemic penumbra as possible. Cerebrovascular autoregulatory mechanisms become impaired in this population; hence CBF becomes dependent on cerebral perfusion pressure. Clinically, a real-time bedside monitor of CBF is not available.

Current guidelines recommend an empirical technique, whereby the head-of-bed (HOB) angle is altered; a flat HOB angle is employed in order to maximize CBF following AIS. In a recent study, we monitored cerebral haemodynamics at the bedside when changes were induced in HOB positioning [47,58]. In healthy populations, CBF responses to posture change were shown to be small owing to autoregulation [47]. Figure 7*a* shows CBF measured on the forehead of a healthy subject at different HOB positions of 30°, 15°, 0°, −5° and 0°, and normalized to their values at 30°. Figure 7*b* shows changes in CBF for a stroke patient. Ischaemic stroke disrupts cerebral autoregulation, and the impaired relationship between CBF and perfusion pressure leads to larger changes in CBF in the infarcted hemisphere by comparison with the healthy contralesional hemisphere. A clear differentiation can be observed between the two hemispheres. This difference was statistically significant over the whole population. On the other hand, approximately 20 per cent of the patients exhibited a paradoxical response, wherein CBF in the ipsilesional hemisphere decreased with increasing HOB angle (figure 7*c*). This behaviour was also previously observed in traumatic brain injury patients and was probably a result of a substantial increase in intracranial pressure—a parameter that is not routinely monitored in ischaemic

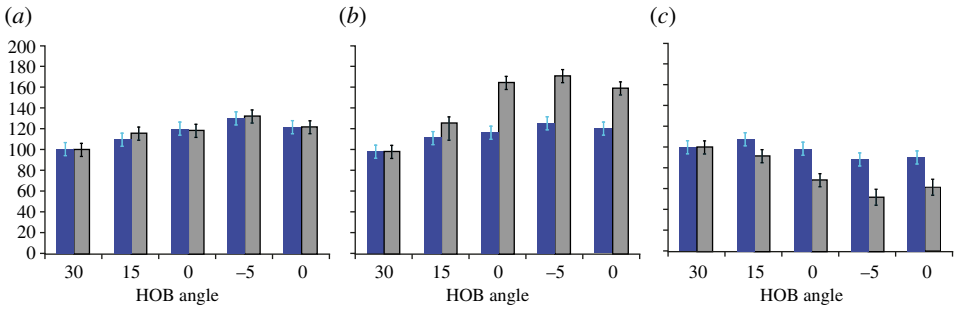

Figure 7. (*a*) CBF changes in each hemisphere (left, blue bars; right, grey bars) after HOB angle manipulation in a healthy subject. CBF changes in a diseased population exhibited (*b*) impaired autoregulation in the injured hemisphere, but about 20% of the population presented a (*c*) paradoxical response, wherein CBF decreased at −5°. (*b*,*c*) Blue bars, contralesional; grey bars, ipsilesional. (Online version in colour.)

stroke patients. Thus, this example illustrates the potential of DCS as a bedside CBF monitor of critically ill patients, which may also allow changes in CBF and metabolism to be detected prior to the onset of clinical symptoms.

Another clinical example concerns haemodynamic monitoring of tumour responses to treatment, especially during the early stages of therapy. The feasibility of DCS/NIRS for this type of application in humans has been demonstrated for breast [33,36,38], head and neck tumours [34,37] and for basal cell carcinomas [39]. The early flow changes that were found may be significant in affecting drug-delivery efficacy and/or tumour oxygenation during chemoradiation therapy.

As a final example, we describe a recent pre-clinical investigation of the utility of DCS for gene-expression studies during the angiogenesis process in murine models [50]. After ligation of the femoral artery in mice, the limb displays a severe decrease in blood flow; generally the flow drops to less than 20 per cent of the flow in the contralateral limb. In reaction to this ischaemia, a vascular response develops that is marked by the formation of new blood vessels in the thigh and calf muscles. We used DCS to assess perfusion in both the occluded and non-occluded limbs before and after femoral artery ligation. Mice were followed periodically for four weeks after surgery in order to track the revascularization process initiated by angiogenesis. Mice with the transcription factor HIF-2α deleted (KO mice) were evaluated relative to control mice; this gene is known to be activated in hypoxic conditions, although its role affecting angiogenesis development is still unknown. After inducing the same level of limb ischaemia in both types of animals, we found that KO mice recovered significantly less than control mice, with the former reaching a steady-state level at approximately 55 per cent of the initial flow levels (i.e. 55% of the ratio measured before femoral artery occlusion). This recovery in perfusion can be attributed to the new vascular network formed after occlusion, where new blood vessels are formed to overcome hypoxia. This result established diffuse optics as a non-invasive and practical method to evaluate the role of transcription factors in mice physiology during angiogenesis.

5. Some limitations of diffuse correlation spectroscopy

Although the field is increasingly oriented towards understanding dynamic processes in the body and related clinical applications, as described in the previous sections, important fundamental issues about the technique remain and deserve attention. At the most basic level, for example, the reason for why the dynamics of RBCs are so well approximated by a Brownian motion flow model is still not clear. In principle, one expects that the distribution of velocities of the RBCs to be macroscopically isotropic and not ballistic, but a rigorous theoretical justification for observations (figure 1) is desired. The solution might depend on assumptions about spatial as well as temporal properties of the vasculature.

In a different vein, motion artefacts, generated by the relative movement of 'static' scatterers with respect to optical fibres, are common and can generate signals that can mislead physiological interpretation. This problem is especially important for exercise experiments. While some progress has been made towards decreasing the magnitude of this problem by time-gating the measurements [31], a detailed analysis is needed to learn better how motion artefacts affect the signal and/or how assumptions in analysis schemes may be violated, when motion artefacts are present [32]. The influence of optical probe pressure is another important parameter that has yet to be fully considered. In brain experiments, for example, the pressure between the probe and the scalp can alter blood flow indices; in muscle experiments, increased pressure may squeeze blood out of the region probed.

On the instrumentation side, the low SNR levels in human brain experiments, mainly owing to higher absorption in the brain and the use of small diameter single-mode fibres, are also challenging. Methods to overcome this problem include placement of many detection fibres around the same region for parallel detection (i.e. effectively increased detection area). Another difficulty faced by many probes on the brain is the presence of hair (especially dark hair) on the scalp that reduces collection efficiency, among other things.

In general, improved theory and improved instrumentation should ameliorate some of the issues outlined above. Feedback from clinical experience will also inform the field. In brain monitoring, for example, it is clear that information about tissue morphology (e.g. skull and scalp geometry) combined with measurement and analysis will be useful for improving the probe fidelity.

6. Summary

In this paper, we described a variety of applications for diffuse optics (particularly DCS) spanning from small animals to humans. The technique has been validated as a reliable, portable and continuous monitor to quantitatively assess microvascular blood flow changes in biological tissue (see table 1 for a list of validation studies). Although the technique is not fully understood yet, many theoretical and experimental improvements have contributed to the advancement of the DCS. This progress has enabled clinical translation of the technique, and has permitted experiments aiming to improve patient care and in pre-clinical contexts. To summarize, we are living through an exciting time for diffuse optics in general, and tissue blood flow measurements in particular! Interested readers

are strongly encouraged to try out these ideas in their laboratories and to consult primary references and recent reviews for more detailed discussion of these topics.

The authors are happy to acknowledge many fruitful discussions and interactions over the years with colleagues from the biomedical community at the University of Pennsylvania and, indeed, throughout the world. At the University of Pennsylvania, most of our blood flow research has been facilitated by sustained collaborations with Britton Chance, Joel Greenberg, John Detre, Theresa Busch, Thomas Floyd, Andrew Kofke, Daniel Licht, David Boas and Joseph Culver. A.G.Y. is indebted to Britton Chance for his inspiration, insight and example over the last 20 odd years. He will be dearly missed. This work was supported by the National Institute of Health through NS-060653, HL-57835, RR-02305, NS-45839 and CA-126187.

References

1 Durduran, T., Choe, R., Baker, W. B. & Yodh, A. G. 2010 Diffuse optics for tissue monitoring and tomography. *Rep. Prog. Phys.* **73**, 076701. (doi:10.1088/0034-4885/73/7/076701)
2 Yodh, A. G. & Boas, D. A. 2003 *Functional imaging with diffusing light*. Boca Raton, FL: CRC Press.
3 Mesquita, R. C. & Yodh, A. G. 2011 Diffuse optics: fundamentals and tissue applications. In *Nano optics and atomics: transport of light and matter waves* (eds R. Kaiser, D. S. Wiersma & L. Fallani). Proceedings of the International School of Physics 'Enrico Fermi', vol. 173. Amsterdam, The Netherlands: IOS Books.
4 Yodh, A. G. & Chance, B. 1995 Spectroscopy and imaging with diffusing light. *Phys. Today* **48**, 34–40. (doi:10.1063/1.881445)
5 Berne, B. J. & Pecora, R. 1990 *Dynamic light scattering with applications to chemistry, biology, and physics*. New York, NY: Krieger.
6 Chu, B. 1991 *Laser light scattering: basic principles and practice*. New York, NY: Academic Press.
7 Clark, N. A., Lunacek, J. H. & Benedek, G. B. 1970 A study of Brownian motion using light scattering. *Am. J. Phys.* **38**, 575–585. (doi:10.1119/1.1976408)
8 Van de Hulst, H. C. 1981 *Light scattering by small particles*. New York, NY: Dover.
9 Boas, D. A., Campbell, L. E. & Yodh, A. G. 1995 Scattering and imaging with diffusing temporal field correlations. *Phys. Rev. Lett.* **75**, 1855–1858. (doi:10.1103/PhysRevLett.75.1855)
10 Boas, D. A. & Yodh, A. G. 1997 Spatially varying dynamical properties of turbid media probed with diffusing temporal light correlation. *J. Opt. Soc. Am. A* **14**, 192–215. (doi:10.1364/JOSAA.14.000192)
11 Maret, G. & Wolf, P. E. 1987 Multiple light scattering from disordered media. The effect of Brownian motion of scatterers. *Z. Phys. B* **65**, 409–413. (doi:10.1007/BF01303762)
12 Stephen, M. J. 1988 Temporal fluctuations in wave propagation in random media. *Phys. Rev. B* **37**, 1–5. (doi:10.1103/PhysRevB.37.1)
13 Pine, D. J., Weitz, D. A., Chaikin, P. M. & Herbolzheimer, E. 1988 Features of diffusing wave spectroscopy. *Phys. Rev. Lett.* **60**, 1134–1137. (doi:10.1103/PhysRevLett.60.1134)
14 Lemieux, P. A. & Durian, D. J. 1999 Investigating non-Gaussian scattering processes by using nth-order intensity correlation functions. *J. Opt. Soc. Am. A* **16**, 1651–1664. (doi:10.1364/JOSAA.16.001651)
15 Strangman, G., Franceschini, M. A. & Boas, D. A. 2003 Factors affecting the accuracy of near-infrared spectroscopy concentration calculations for focal changes in oxygenation parameters. *Neuroimage* **18**, 865–879. (doi:10.1016/S1053-8119(03)00021-1)
16 Takeda, H., Tomita, M., Tanahashi, N., Kobari, M., Takao, M. & Amano, T. 2004 Light scattering by blood: pitfalls in measurement of cerebral hemoglobin concentration. *Jpn. J. Cereb. Blood Flow Metab.* **16**, 295–296.
17 Tomita, M. 2006 Flow effect impacts NIRS, jeopardizing quantification of tissue hemoglobin. *Neuroimage* **33**, 13–16. (doi:10.1016/j.neuroimage.2006.06.046)

18 Cheung, C., Culver, J. P., Takahashi, K., Greenberg, J. H. & Yodh, A. G. 2001 *In vivo* cerebrovascular measurement combining diffuse near-infrared absorption and correlation spectroscopies. *Phys. Med. Biol.* **46**, 2053–2065. (doi:10.1088/0031-9155/46/8/302)

19 Culver, J. P., Durduran, T., Furuya, D., Cheung, C., Greenberg, J. H. & Yodh, A. G. 2003 Diffuse optical tomography of cerebral blood flow, oxygenation and metabolism in rat during focal ischemia. *J. Cereb. Blood Flow Metab.* **23**, 911–924. (doi:10.1097/01.WCB.0000076703.71231.BB)

20 Zhou, C., Yu, G., Furuya, D., Greenberg, J. H., Yodh, A. G. & Durduran, T. 2006 Diffuse optical correlation tomography of cerebral blood flow during cortical spreading depression in rat brain. *Opt. Express* **14**, 1125–1144. (doi:10.1364/OE.14.001125)

21 Culver, J. P., Durduran, T., Cheung, C., Furuya, D., Greenberg, J. H. & Yodh, A. G. 2003 Diffuse optical measurement of hemoglobin and cerebral blood flow in rat brain during hypercapnia, hypoxia and cardiac arrest. *Adv. Exp. Med. Biol.* **510**, 293–297.

22 Carp, S. A., Dai, G. P., Boas, D. A., Franceschini, M. A. & Kim, Y. R. 2010 Validation of diffuse correlation spectroscopy measurements of rodent cerebral blood flow with simultaneous arterial spin labeling MRI; towards MRI-optical continuous cerebral metabolic monitoring. *Biomed. Opt. Express* **1**, 553–565. (doi:10.1364/BOE.1.000553)

23 Busch, T. M., Xing, X., Yu, G., Yodh, A., Wileyto, E. P., Wang, H. W., Durduran, T., Zhu, T. C. & Wang, K. K. H. 2009 Fluence rate-dependent intratumor heterogeneity in physiologic and cytotoxic responses to photofrin photodynamic therapy. *Photochem. Photobiol. Sci.* **8**, 1683–1693. (doi:10.1039/b9pp00004f)

24 Sunar, U., Makonnen, S., Zhou, C., Durduran, T., Yu, G., Wang, H. W., Lee, W. M. & Yodh, A. G. 2007 Hemodynamic responses to antivascular therapy and ionizing radiation assessed by diffuse optical spectroscopies. *Opt. Express* **15**, 15 507–15 516. (doi:10.1364/OE.15.015507)

25 Yu, G. *et al.* 2005 Noninvasive monitoring of murine tumor blood flow during and after photodynamic therapy provides early assessment of therapeutic efficacy. *Clin. Cancer Res.* **11**, 3543–3552. (doi:10.1158/1078-0432.CCR-04-2582)

26 Menon, C. *et al.* 2003 An integrated approach to measuring tumor oxygen status using human melanoma xenografts as a model. *Cancer Res.* **63**, 7232–7240.

27 Zhou, C., Eucker, S., Durduran, T., Yu, G., Ralston, J., Friess, S. H., Ichord, R. N., Margulies, S. S. & Yodh, A. G. 2009 Diffuse optical monitoring of hemodynamic changes in piglet brain with closed head injury. *J. Biomed. Opt.* **14**, 034015. (doi:10.1117/1.3146814)

28 Yu, G., Durduran, T., Lech, G., Zhou, C., Chance, B., Mohler, E. R. & Yodh, A. G. 2005 Time-dependent blood flow and oxygenation in human skeletal muscle measured with noninvasive near-infrared diffuse optical spectroscopies. *J. Biomed. Opt.* **10**, 024027. (doi:10.1117/1.1884603)

29 Yu, G., Floyd, T., Durduran, T., Zhou, C., Wang, J. J., Detre, J. A. & Yodh, A. G. 2007 Validation of diffuse correlation spectroscopy for muscle blood flow with concurrent arterial spin labeled perfusion MRI. *Opt. Express* **15**, 1064–1075. (doi:10.1364/OE.15.001064)

30 Shang, Y., Zhao, Y., Cheng, R., Dong, L., Irwin, D. & Yu, G. 2009 Portable optical tissue flow oximeter based on diffuse correlation spectroscopy. *Opt. Lett.* **34**, 3556–3558. (doi:10.1364/OL.34.003556)

31 Shang, Y., Symons, T. B., Durduran, T., Yodh, A. G. & Yu, G. 2010 Effects of muscle fiber motion on diffuse correlation spectroscopy blood flow measurements during exercise. *Biomed. Opt. Express* **1**, 500–511. (doi:10.1364/BOE.1.000500)

32 Belau, M., Ninck, M., Hering, G., Spinelli, L., Contini, D., Torricelli, A. & Gisler, T. 2010 Noninvasive observation of skeletal muscle contraction using near-infrared time-resolved reflectance and diffusing wave spectroscopy. *J. Biomed. Opt.* **15**, 057007. (doi:10.1117/1.3503398)

33 Durduran, T., Choe, R., Yu, G., Zhou, C., Tchou, J. C., Czerniecki, B. J. & Yodh, A. G. 2005 Diffuse optical measurement of blood flow in breast tumors. *Opt. Lett.* **30**, 2915–1917. (doi:10.1364/OL.30.002915)

34 Sunar, U. *et al.* 2006 Noninvasive diffuse optical measurement of blood flow and blood oxygenation for monitoring radiation therapy in patients with head and neck tumors: a pilot study. *J. Biomed. Opt.* **11**, 064021. (doi:10.1117/1.2397548)

35 Yu, G., Durduran, T., Zhou, C., Zhu, T. C., Finlay, J. C., Busch, T. M., Malkowicz, S. B., Hahn, S. M. & Yodh, A. G. 2006 Real-time *in situ* monitoring of human prostate photodynamic therapy with diffuse light. *Photochem. Photobiol.* **82**, 1279–1284. (doi:10.1562/2005-10-19-RA-721)

36 Zhou, C. *et al.* 2007 Diffuse optical monitoring of blood flow and oxygenation in human breast cancer during early stages of neoadjuvant chemotherapy. *J. Biomed. Opt.* **12**, 051903. (doi:10.1117/1.2798595)

37 Sunar, U., Rohrbach, D., Rigual, N., Tracy, E., Keymel, K., Cooper, M. T., Baumann, H. & Henderson, B. H. 2010 Monitoring photobleaching and hemodynamic responses to HPPH-mediated photodynamic therapy of head and neck cancer: a case report. *Opt. Express* **18**, 14969–14978. (doi:10.1364/OE.18.014969)

38 Choe, R. *et al.* 2009 Differentiation of benign and malignant breast tumors by *in-vivo* three-dimensional parallel-plate diffuse optical tomography. *J. Biomed. Opt.* **14**, 024020. (doi:10.1117/1.3103325)

39 Becker, T. L., Paquette, A. D., Keymel, K. R., Henderson, B. W. & Sunar, U. 2011 Monitoring blood flow responses during topical ALA-PDT. *Biomed. Opt. Express* **2**, 123–130. (doi:10.1364/BOE.2.000123)

40 Durduran, T., Yu, G., Burnett, M. G., Detre, J. A., Greenberg, J. H., Wang, J., Zhou, C. & Yodh, A. G. 2004 Diffuse optical measurements of blood flow, blood oxygenation and metabolism in human brain during sensorimotor cortex activation. *Opt. Lett.* **29**, 1766–1768. (doi:10.1364/OL.29.001766)

41 Li, J., Dietsche, G., Iftime, D., Skipetrov, S. E., Maret, G., Elbert, T., Rockstroh, B. & Gisler, T. 2005 Noninvasive detection of functional brain activity with near-infrared diffusing-wave spectroscopy. *J. Biomed. Opt.* **10**, 044002. (doi:10.1117/1.2007987)

42 Jaillon, F., Li, J., Dietsche, G., Elbert, T. & Gisler, T. 2007 Activity of the human visual cortex measured noninvasively by diffusing-wave spectroscopy. *Opt. Express* **15**, 6643–6650. (doi:10.1364/OE.15.006643)

43 Dietsche, G., Ninck, M., Ortolf, C., Li, J., Jaillon, F. & Gisler, T. 2007 Fiber-based multispeckle detection for time-resolved diffusing-wave spectroscopy: characterization and application to blood flow detection in deep tissue. *App. Opt.* **46**, 8506–8514. (doi:10.1364/AO.46.008506)

44 Li, J., Ninck, M., Koban, L., Elbert, T., Kissler, J. & Gisler, T. 2008 Transient functional blood flow change in the human brain measured noninvasively by diffusing-wave spectroscopy. *Opt. Lett.* **33**, 2233–2235. (doi:10.1364/OL.33.002233)

45 Koban, L., Ninck, M., Li, J., Gisler, T. & Kissler, J. 2010 Processing of emotional words measured simultaneously with steady-state visually evoked potentials and near-infrared diffusing-wave spectroscopy. *BMC Neurosci.* **11**, 85. (doi:10.1186/1471-2202-11-85)

46 Zirak, P., Delgado-Mederos, R., Martí-Fàbregas, J. & Durduran, T. 2010 Effects of acetazolamide on the micro- and macro-vascular cerebral hemodynamics: a diffuse optical and transcranial Doppler ultrasound study. *Biomed. Opt. Express* **1**, 1443–1459. (doi:10.1364/BOE.1.001443)

47 Edlow, B. L., Kim, M. N., Durduran, T., Zhou, C., Putt, M. E., Yodh, A. G., Greenberg, J. H. & Detre, J. A. 2010 The effects of healthy aging on cerebral hemodynamic responses to posture change. *Physiol. Meas.* **31**, 477–495. (doi:10.1088/0967-3334/31/4/002)

48 Roche-Labarbe, N., Carp, S. A., Surova, A., Patel, M., Boas, D. A., Grant, P. E. & Franceschini, M. A. 2010 Noninvasive optical measures of CBV, $S_tO(2)$, CBF index, and rCMRO(2) in human premature neonates' brains in the first six weeks of life. *Hum. Brain Mapp.* **31**, 341–352. (doi:10.1002/hbm.20868)

49 Einstein, A. 1905 On the motion of small particles suspended in liquids at rest required by the molecular-kinetic theory of heat. *Ann. Phys.* **17**, 549–560. (doi:10.1002/andp.19053220806)

50 Mesquita, R. C., Skuli, N., Kim, M. N., Liang, J., Schenkel, S., Majmundar, A. J., Simon, M. C. & Yodh, A. G. 2010 Hemodynamic and metabolic diffuse optical monitoring in a mouse model of hindlimb ischemia. *Biomed. Opt. Express* **1**, 1173–1187. (doi:10.1364/BOE.1.001173)

51 Durduran, T. 2004 Non-invasive measurements of tissue hemodynamics with hybrid diffuse optical methods. PhD dissertation, University of Pennsylvania, PA, USA.

52 Durduran, T. *et al.* 2010 Optical measurement of cerebral hemodynamics and oxygen metabolism in neonates with congenital heart defects. *J. Biomed. Opt.* **15**, 037004. (doi:10.1117/1.3425884)
53 Buckley, E. M. *et al.* 2009 Cerebral hemodynamics in preterm infants during positional intervention measured with diffuse correlation spectroscopy and transcranial Doppler ultrasound. *Opt. Express* **17**, 12571–12581. (doi:10.1364/OE.17.012571)
54 Kim, M. N. *et al.* 2010 Noninvasive measurement of cerebral blood flow and blood oxygenation using near-infrared and diffuse correlation spectroscopies in critically brain-injured adults. *Neurocrit. Care* **12**, 173–180. (doi:10.1007/s12028-009-9305-x)
55 Patterson, M. S., Andersson-Engels, S., Wilson, B. C. & Osei, E. K. 1995 Absorption spectroscopy in tissue-simulating materials: a theoretical and experimental study of photon paths. *App. Opt.* **34**, 22–30. (doi:10.1364/AO.34.000022)
56 Kuebler, W. M., Sckell, A., Habler, O., Kleen, M., Kuhnle, G. E. H., Welte, M., Messmer, K. & Goetz, A. E. 1998 Noninvasive measurement of regional cerebral blood flow by near-infrared spectroscopy and indocyanine green. *J. Cereb. Blood Flow Metab.* **18**, 445–456. (doi:10.1097/00004647-199804000-00013)
57 Terborg, C., Groschel, K., Petrovitch, A., Ringer, T., Schnaudigel, S., Witte, O. W. & Kastrup, A. 2009 Noninvasive assessment of cerebral perfusion and oxygenation in acute ischemic stroke by near-infrared spectroscopy. *Eur. Neurol.* **62**, 338–343. (doi:10.1159/000239794)
58 Durduran, T. *et al.* 2009 Transcranial optical monitoring of cerebrovascular hemodynamics in acute stroke patients. *Opt. Express* **17**, 3884–3902. (doi:10.1364/OE.17.003884)
59 Mayhew, J., Johnston, D., Martindale, J., Jones, M., Berwick, J. & Zheng, Y. 2001 Increased oxygen consumption following activation of brain: theoretical footnotes using spectroscopic data from barrel cortex. *Neuroimage* **13**, 975–987. (doi:10.1006/nimg.2001.0807)
60 Boas, D. A., Strangman, G., Culver, J. P., Hoge, R. D., Jasdzewski, G., Poldrack, R. A., Rosen, B. R. & Mandeville, J. B. 2003 Can the cerebral metabolic rate of oxygen be estimated with near-infrared spectroscopy? *Phys. Med. Biol.* **48**, 2405–2418. (doi:10.1088/0031-9155/48/15/311)
61 Bandettini, P. A., Wong, E. C., Hinks, R. S., Tikofsky, R. S. & Hyde, J. S. 1992 Time course EPI of human brain function during task activation. *Magn. Reson. Med.* **25**, 390–397. (doi:10.1002/mrm.1910250220)
62 Hoge, R. D., Franceschini, M. A., Covolan, R. J. M., Huppert, T., Mandeville, J. B. & Boas, D. A. 2005 Simultaneous recording of task-induced changes in blood oxygenation, volume, and flow using diffuse optical imaging and arterial spin-labeling MRI. *Neuroimage* **25**, 701–707. (doi:10.1016/j.neuroimage.2004.12.032)
63 Hatazawa, J., Sasajima, T., Shimosegawa, E., Fujita, H., Okudera, T., Kanno, I., Mineura, K. & Uemura, K. 1996 Regional cerebral blood flow response in gray matter heterotopia during finger tapping: an activation study with positron emission tomography. *AJNR Am. J. Neuroradiol.* **17**, 479–482.